arXiv:1210.5920v2 [physics.bio-ph] 11 Dec 2012

Malaria pigment crystals as magnetic micro-rotors: key for high-sensitivity diagnosis

A. Butykai,[1] A. Orbán,[1] V. Kocsis,[1] D. Szaller,[1] S. Bordács,[1] E. Tátrai-Szekeres,[1]
L.F. Kiss,[2] A. Bóta,[3] B.G. Vértessy,[4,5] T. Zelles,[6] and I. Kézsmárki*[1]

[1]*Department of Physics, Budapest University of Technology and Economics and Condensed Matter Research Group of the Hungarian Academy of Sciences, H-1111 Budapest, Hungary*
[2]*Institute for Solid State Physics and Optics, Wigner Research Centre for Physics, Hungarian Academy of Sciences, H-1525 Budapest, Hungary*
[3]*Department of Biological Nanochemistry, Institute of Molecular Pharmacology, Research Center for Natural Sciences, Hungarian Academy of Sciences, H-1025 Budapest, Hungary*
[4]*Institute of Enzymology, Research Center for Natural Sciences, Hungarian Academy of Sciences, H-1113 Budapest, Hungary*
[5]*Department of Applied Biotechnology and Food Science, Budapest University of Technology and Economics, H-1111 Budapest, Hungary*
[6]*Department of Oral Biology, Semmelweis University, H-1089 Budapest, Hungary*

(Dated: December 12, 2012)

The need to develop new methods for the high-sensitivity diagnosis of malaria has initiated a global activity in medical and interdisciplinary sciences. Most of the diverse variety of emerging techniques are based on research-grade instruments, sophisticated reagent-based assays or rely on expertise. Here, we suggest an alternative optical methodology with an easy-to-use and cost-effective instrumentation based on unique properties of malaria pigment reported previously and determined quantitatively in the present study. Malaria pigment, also called hemozoin, is an insoluble microcrystalline form of heme. These crystallites show remarkable magnetic and optical anisotropy distinctly from any other components of blood. As a consequence, they can simultaneously act as magnetically driven micro-rotors and spinning polarizers in suspensions. These properties can gain importance not only in malaria diagnosis and therapies, where hemozoin is considered as drug target or immune modulator, but also in the magnetic manipulation of cells and tissues on the microscopic scale.

In spite of the global efforts made for its elimination including preventive strategies and drug therapies, malaria is still the topmost vector-borne infectious disease with more than 200 million clinical cases and around 1 million fatalities a year[1]. Increasing drug resistance of the parasites strongly acts against the global malaria control, while climate change can even result in the reintroduction of malaria mosquitos into post-endemic countries. A significant improvement could be achieved via the development of cheap diagnostic methods accurate even at the early stage of the infection and via new drugs or vaccines efficient against the most severe types of malaria parasites[2,3].

Among diagnostic methods currently in practice the most reliable and sensitive one is the microscopic observation of blood smears –able to detect parasitemia associated with 5-10 parasites in $1\,\mu$l blood–, which is rather costly as requiring expertise and high-powered microscopes. Though antigen-based detection of malaria parasites offers a cheaper alternative and the corresponding rapid diagnostic tests (RDT) are widely used[4–6], presently these techniques have strong limitations. Perhaps the two major drawbacks are that i) RDTs are not sensitive enough to detect early-stage infections, the current sensitivity threshold being around $100\,\text{parasites}/\mu\text{l}$ and ii) the tests are not quantitative enough to distinguish between levels of infections (in endemic areas, most individuals will test positive showing some degree of parasitemia but not allowing identification of patients with active disease requiring urgent treatment)[7]. Additionally, false positive results may arise due to the imperfect clearage of antigen proteins from the body after successful treatments, while false negative results are owing to their absence in certain Plasmodium strains[8], as is the case for histidine-rich protein II[9]. Although among the molecular biology-based methods, polymerase chain reaction (PCR) assays are sensitive enough to detect 1 parasite $/\mu$l[10,11], the practical use of PCR assays on the field is limited due to requirements of sophisticated technology and expertise.

In the last few years, the need to develop new diagnostic methods has been driving extended research and a large arsenal of diagnostic schemes has been proposed. Some of them are still based on selective microscopic detection of infected blood cells such as magnetic deposition microscopy[12], third harmonic generation imaging[13], fluorescent study of cell microarray chips[14] and photoacoustic flowmetry[15]. There is an increasing number of methods using malaria pigment as the target material for magnetic diagnosis including magnetic purification processes[12,16], magneto-optical detection using polarized light[17], electrochemical magneto immunosensors[19] and magnetic field enriched surface enhanced resonance Raman spectroscopy[20].

Malaria pigment, also called hemozoin, is a byproduct of the disease formed during the intraerythrocytic growth cycle of the parasites[21,22]. Digestion of hemoglobin by the malaria parasites results in the accumulation of monomeric heme. As it is highly toxic to the parasites, they transform heme into an insoluble crystal-

Typeset by REVTEX

lized form in which heme groups are dimerized through ironcarboxylate links and the three dimensional structure is stabilized via hydrogen bonds[23]. This process is accompanied by the change in the valency and the local coordination of iron and leads to the transformation of low-spin diamagnetic Fe^{2+} ions contained in oxyhemoglobin into high-spin (S=5/2) paramagnetic Fe^{3+} ions in hemozoin[24–26]. Besides playing a key role in several diagnostic techniques, malaria pigment, an ensemble of submicron-sized paramagnetic hemozoin crystallites, is a main drug target and may also act as an immune modulator[27,28].

Hemozoin has a low-symmetry triclinic crystal structure[29] as shown in Fig. 1a. Although the morphology of the crystallites shows variations depending on the parasite species[30,31], they typically have an elongated rod-like shape with a length ranging from 300 nm to 1 μm. Besides the natural formation of hemozoin inside the parasites, various methods have been established for its chemical synthesis[23,32]. Though the artificially grown version is usually called β-hematin to be distinguished from hemozoin, they are demonstrated to share identical chemical composition, crystal structure[23,29], optical[23,33] and magnetic properties[24,25]. Hereafter, we will refer to both natural and synthetic versions of malaria pigment as hemozoin. Hemozoin crystals used in the present study were prepared from hemin by an aqueous acid-catalyzed reaction[28]. Transmission electron micrograph (TEM) images of typical crystallites are shown in Fig. 1c. Similarly to the naturally grown ones, they are elongated and characterized by a size distribution of $\sim$700$\pm$200 nm.

Here, by extending the work of Newman and coworkers[17] we report a new path for the magnetic detection of malaria, which, in contrast to most of the aforementioned recently emerging techniques, may be realized as a cheap and compact diagnostic tool without the application of research-grade instruments. Unique magnetic and optical properties of malaria pigment crystals as well as their highly controllable dynamics in fluids, which all play key roles in the principle of detection, are systematically investigated. The threshold of our device detecting hemozoin content, as in the present trial state, is 15 picogram of hemozoin in 1 μl blood equivalent to a level of parasitemia $\lesssim$30 parasites/μl[17], which needs to be confirmed via extended clinical trials. While this detection limit already shows improvement over that of RDTs, it is further decreased by about more than one order of magnitude for hemozoin detection in blood plasma or serum corresponding to a parasitemia less than 1 parasite/μl.

Results

The diagnostic methodology presented in this paper relies to a large extent on magnetic properties which are highly specific to malaria pigment crystals and unique in human body. First we review the fundamental characteristics of the crystallites determined by magnetization and magneto-optical measurements. The following part describes the dynamics of their magnetically driven rotation in fluids with different viscosity such as hemolyzed blood, water, acetone, etc.

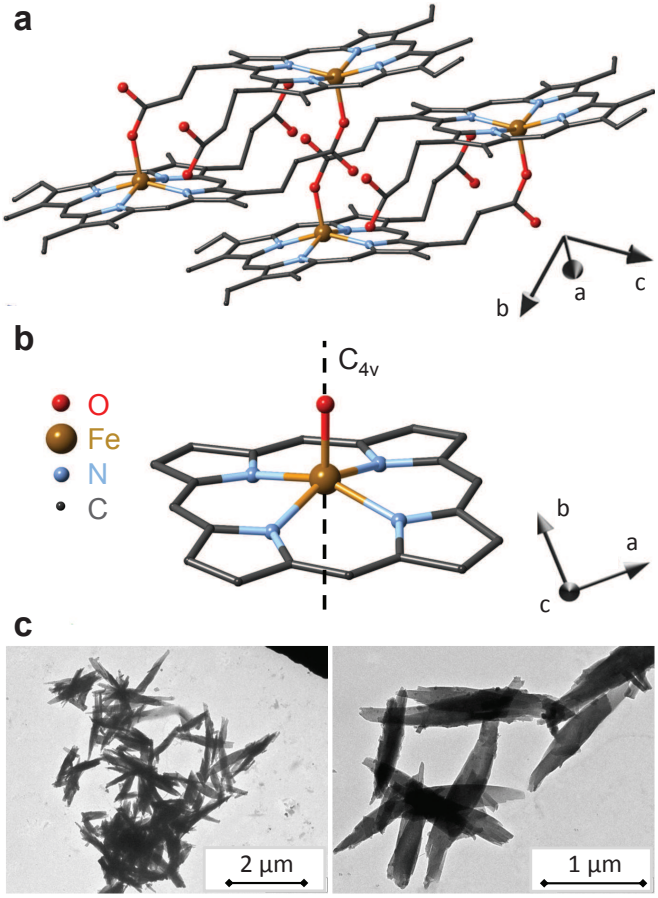

FIG. 1: | **Structure and morphology of hemozoin crystals.** (**a**) Triclinic structure of hemozoin with two unit cells displayed using structural data from Ref. 29. The main crystallographic axes a, b and c are also indicated. (**b**) The local symmetry of five-fold coordinated iron in hemozoin nearly preserves a four-fold rotation axis, C_{4v}. The angle spanned by this C_{4v} axis (hard axis of the magnetization) and the crystallographic c-axis (fore-axis of the elongated crystals) is $\delta\approx 60^o$, where the c-axis points out of the plane of the figure. (**c**) Transmission electron micrographs of typical hemozoin crystallites dried from suspensions.

Magnetic anisotropy of hemozoin. The low crystal symmetry would generally imply that hemozoin is a highly anisotropic paramagnet with different magnetic susceptibility values along each of the three main crystallographic axes. However, Fe^{3+} ions located in the center of porphyrin rings experience higher local symmetry since the four-fold rotational axis perpendicular to the plane of the porphyrin unit is nearly preserved as shown in Figs. 1a-b. Therefore, we expect that the magnetic properties of malaria pigment, which are mainly determined by Fe^{3+} ions, reflect this axial (C_{4v}) symmetry

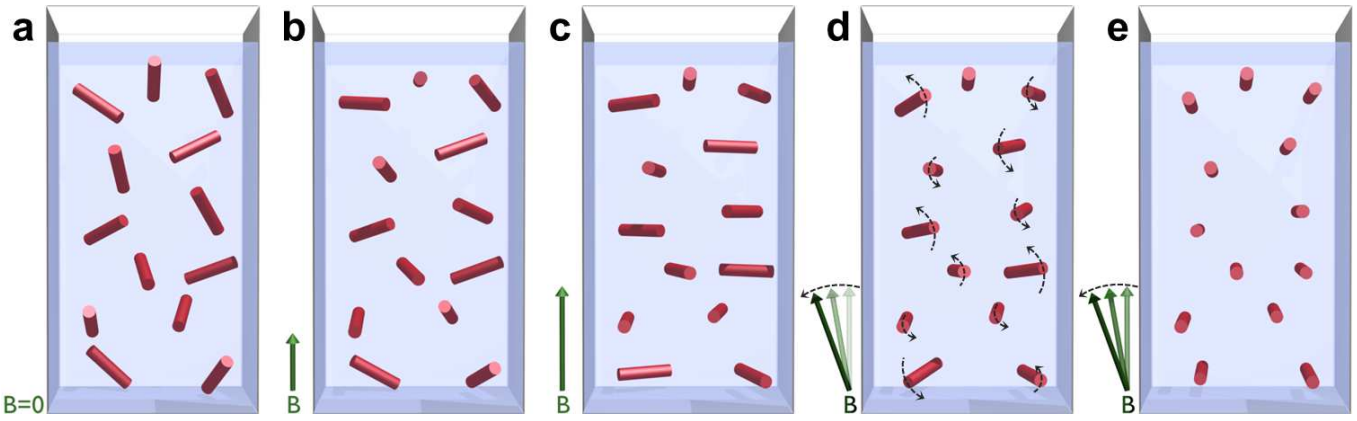

FIG. 2: | **Magnetic orientation and dynamics of paramagnetic hemozoin crystals with anisotropic easy-plane character.** In these schematic drawings, the cylinders represent the suspended hemozoin crystals. The axes of the cylinders correspond to the magnetic hard axes of the crystals and not related to their fore-axes. (**a**) Without external magnetic field the crystals in the suspension are randomly oriented. (**b**) With the application of a magnetic field, the hard axes of the crystals begin to align perpendicular to the magnetic field vector **B**, though this orientation is hindered by the thermal fluctuations. (**c**) In the high-field limit this two-dimensional alignment is completed, with the hard axis of each crystal lying within the plane normal to the field. (**d**) In slowly rotating fields the crystallites behave as magnetically driven micro-rotors. (**e**) Due to the viscosity of the fluid, at high rotation frequencies their hard axes tend to align parallel to the rotation axis and consequently they stop spinning. Only in this case a full three dimensional alignment of the hard axes is achieved.

and hemozoin behaves either as an easy-axis or as an easy-plane paramagnet.

Based on a multi-frequency high-field electron paramagnetic resonance (EPR) study on powder samples, Sienkiewitz and co-workers[25] suggested that the behaviour of the S=5/2 spins of Fe^{3+} ions in hemozoin can be described by the following Hamiltonian, $H = D\left(S_z^2 - \frac{S(S+1)}{3}\right) + E(S_x^2 - S_y^2) + \mu_B g\mathbf{BS}$, where D in the first term is the zero-field splitting associated with an axial anisotropy, while lowering of the C_{4v} symmetry introduced via E is negligible as $|E/D| \leq 0.035$. They also found that the Zeemann-splitting induced by an external magnetic field, **B**, is characterized by a nearly isotropic g-factor, g≈2. The dominance of the D term together with its positive sign found in this low-temperature EPR study – in agreement with the results obtained by Mössbauer spectroscopy[24] – hint toward the fact that hemozoin can behave as an easy-plane paramagnet over an extended temperature region. According to the local symmetry generated by the ligand field at iron sites, we assign the easy plane of the magnetization with the plane of the porphyrin rings, hence, the hard direction labeled as z-axis in the spin Hamiltonian above coincides with the four-fold rotational axis.

When such easy-plane crystallites suspended in a liquid are exposed to an external magnetic field, they tend to co-align with the field direction to gain magnetic energy (see Figs. 2a-c). Assuming a linear field dependence of the magnetization, which is experimentally confirmed at room temperature, the magnetic anisotropy energy is $U = -\frac{1}{2}\frac{B^2}{\mu_0} cos^2(\theta)(\chi_{zz} - \chi_{xx})V$. Here, χ_{zz} and χ_{xx} stand for the linear magnetic susceptibility of a crystal along the hard axis and within the easy plane, respectively, θ is the angle between the direction of the field and the hard axis of a crystal and V is its volume. Magnetization densities for fields applied within the easy plane and along the hard axis of the crystal are given by $M_x = \chi_{xx}B/\mu_0$ and $M_z = \chi_{zz}B/\mu_0$, respectively. (For details see Methods section.) Since thermal fluctuations try to restore the random orientation, the angular distribution of the crystals over the suspension depends on the relative strength of the magnetic anisotropy energy and the energy scale of thermal fluctuations, k_BT, according to $f(\theta) = \frac{e^{-U/k_BT}}{2\pi \int_0^\pi e^{-U/k_BT} \sin\theta d\theta}$.

In order to directly determine the strength of the magnetic anisotropy we car ried out field- and temperature-dependent magnetization measurements on powder samples of randomly oriented crystals as well as on crystals suspended in a mixture of 70% water and 30% glycerol. In the second case, the measurements were performed both after zero-field cooling for maintaining the random orientation of the crystals in the suspension and after a field cooling process used to magnetically align the crystals and fix them by freezing the mixture. (Fixation occurs below the freezing point of the mixture, T_{fr}≈230 K – see Supplementary Information.) For suspensions with hemozoin content less than 10 μg/μl, the magnetic field of B=5 T used for field cooling from room temperature down to T=2 K was found safely large to achieve high degree of orientation within the suspensions as schematically illustrated in Fig. 2c. This way we could measure the magnetization specific to the case when the magnetic field lies within the easy plane and the hard axis of each crystal is aligned perpendicular to the field.

Here, we note that the magnetic hard axis is roughly parallel to the [131] crystallographic axis, while the

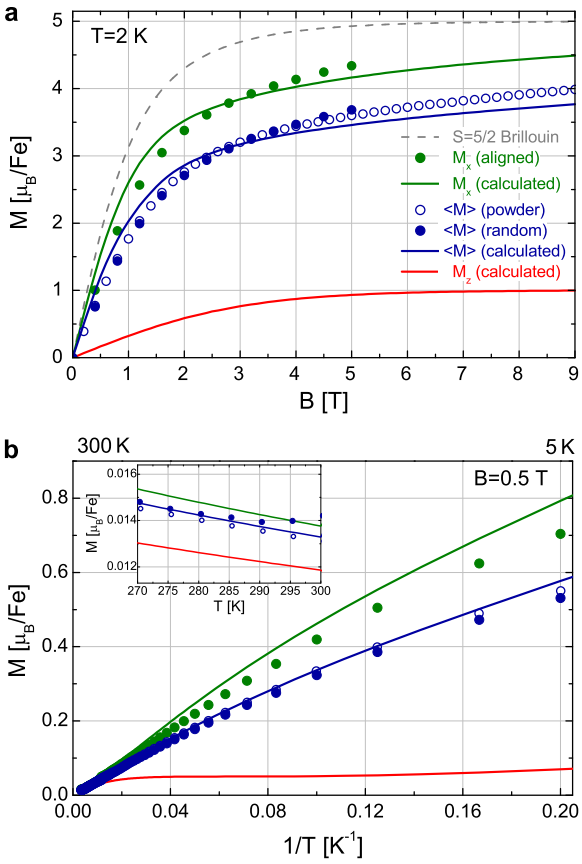

FIG. 3: | **Magnetization anisotropy of malaria pigment crystals.** (**a**) Field dependence of the magnetization measured at T=2 K for a powder sample, randomly oriented (zero-field cooled suspension) crystals and magnetically aligned (field cooled suspension) crystals are shown by blue open circles, blue dots and green dots, respectively. As expected, the former two are essentially identical. Magnetization curves calculated for fields lying within the easy plane and pointing along the hard axis of a crystal are also plotted with green and red lines, respectively. The angular average of the magnetization corresponding to the random orientation of the crystals is also displayed with blue line. (For details of the calculation see the Methods section.) Magnetization values are given for a single iron site in Bohr-magneton units. To emphasize the anisotropic character of hemozoin, Brillouin's function describing the magnetization of an isotropic S=5/2 spin is also shown (dashed grey line). (**b**) Low-field magnetization of hemozoin as a function of the inverse temperature measured in B=0.5 T. The position of 300 K and 5 K are indicated on the upper scale. The inset shows the data on a linear temperature scale around 300 K. Symbols and lines indicate respectively the same measured and calculated quantities as in panel (**a**).

crystallites are elongated along the [001] direction[34,35]. Therefore, the two dimensional co-alignment of the hard axes of the crystals (shown in Fig. 2c) leaves a large freedom for the orientation of their fore-axis since the crystals can rotate around both their hard axes and the direction of the external magnetic field without any change in their magnetic energy. This is in agreement with our TEM observations (see Supplementary Information), which showed that magnetic alignment is not straightforwardly manifested in the orientation of the shape of the crystals, in contrast to former assumptions[17].

The field dependence of the magnetization at T=2 K and the temperature-dependent magnetization measured in B=0.5 T with increasing temperature are plotted in Fig. 3a and 3b, respectively, for powder samples, zero-field cooled and field cooled suspensions. The difference between the magnetization of the randomly oriented and the aligned samples increases with decreasing temperature and clearly shows the anisotropic nature of hemozoin.

To determine the magnetization also for fields pointing along the hard axis of a given crystal from these data, we calculated the magnetization, both as a function of field and temperature, using the spin Hamiltonian with axial anisotropy and tuned the value of D to obtain the best fitting with the measured curves. We found that the magnetization of a crystal strongly depends on the angle θ spanned by its hard axis and the direction of the external field. Besides the magnetization density values corresponding to the easy plane (M_x) and the hard axis (M_z), the magnetization of a sample containing randomly oriented crystals, $\langle M \rangle$, was also evaluated by averaging over θ. All the experimental data shown in Fig. 3 and additional data presented in the Supplementary Information are well reproduced by a common value of the single fitting parameter, D=13.4 K, which is consistent with the value reported in former EPR[25] and Mössbauer[24] spectroscopic studies.

For the anisotropy of the low-field magnetization (or alternatively the linear susceptibility) we obtained a value as large as $M_x/M_z = 9.6 \pm 0.2$ at T=2 K. Though this ratio is gradually reduced when the energy scale of the thermal fluctuations becomes comparable and larger than the zero field splitting, i.e. for $k_B T > D$, it is still considerable at T=300 K with $M_x/M_z \approx 1.16 \pm 0.03$. The magnitude of the anisotropy at room temperature implies that partial (two dimensional) and full (three dimensional) magnetic alignment of the crystals respectively obtained by static and rotating fields can be achieved by magnetic fields of $\lesssim$1 T as proposed in Fig. 2.

Magnetically induced linear dichrosim of malaria pigment. Similarly to the magnetic anisotropy, the planar stacking of Fe^{3+}-protoporphyrin-IX units in hemozoin[29] together with the axial symmetry of iron sites are indicative of anisotropic optical properties for a single crystal (see Figs. 1a-b). More specifically, optical excitations in the absorption spectrum of hemozoin over the near-infrared and the visible regions can be assigned to transitions mainly involving π and π^* orbitals of the porphyrin and d orbitals of the central Fe^{3+} ion[36,37]. These assignments also support the local C_{4v} symmetry of iron in hemozoin similarly to the case of hemin and deoxyhemoglobin[36]. Since the same symmetry dictates the magnetic and optical anisotropy of hemozoin on the

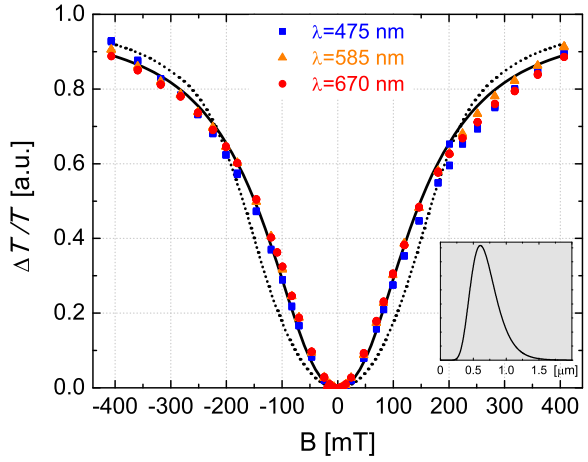

FIG. 4: | **Magnetically induced linear dichroism in hemozoin suspensions.** Magnetic field dependence of linear dichroism measured on a room-temperature aqueous suspension of hemozoin at wavelengths λ =475 nm (blue squares), 585 nm (orange triangles) and 670 nm (red dots). Data corresponding to different wavelengths were normalized to a common scale, which resulted in a universal field dependence reproduced well by the theory. Assuming an average-sized crystal, the fitting (dotted line) yields M_x/M_z=1.11 for the magnetization anisotropy, which corresponds to $M_x - M_z$=0.013 μ_B/Fe in a magnetic field of 5 T. The quality of the fit can be further improved (solid line) by assuming the distribution of crystal size shown in the caption. For details see the main text.

microscopic level, alignment of the crystallites by external field is expected to simultaneously generate macroscopic magnetic and optical anisotropy in their suspensions.

This invokes a diagnostic tool based on magneto-optical phenomena such as magnetically induced linear birefringence/dichroism or polarization dependent light scattering. Though all of these three effects can be relevant we will refer to them as magnetically induced linear dichrosim (MLD). Recently, Newman and coworkers have reported a magneto-optical methodology capable of a sensitive diagnosis of malaria[17,18]. They found a specific field dependence of MLD[38]. In order to probe the microscopic properties of hemozoin we revisited this phenomenon and studied its wavelength dependence.

We investigated the magnetic field dependence of the linear dichroism on aqueous suspensions of hemozoin at multiple wavelengths (e.g. λ=475 nm, 585 nm and 670 nm) by measuring the transmitted intensity in Voigt configuration for light polarizations parallel and perpendicular to the applied field using a polarization modulation technique. (See Methods section for details.) The experimental curves obtained at different wavelengths follow a universal field dependence when normalized to a common scale as shown in Fig. 4. After the quadratic increase of MLD at low fields, the signal tends to saturate with an inflection at an intermediate field $B_0 \approx 0.1$ T.

The mechanism behind MLD in hemozoin suspensions is outlined schematically in Figs. 2a-c. In a dilute suspension the crystals are oriented randomly, resulting in an optically isotropic media since polarization effects from individual crystals average to zero. As already discussed, in external magnetic fields the crystals align in a manner that the field would preferably lie within their easy planes. The ordering is opposed by thermal fluctuations and this competition determines the specific field dependence of MLD. The linear dichroism of a single hemozoin crystal is characterized by the difference of its transmission coefficients T_x and T_z corresponding to light polarizations parallel and perpendicular to the porphyrin planes, respectively. (These directions were respectively called easy plane and hard axis in the former magnetic terminology.) In external magnetic field the contributions from individual crystals produce a macroscopic transmission anisotropy between polarizations parallel and perpendicular to the field direction

$$\frac{\Delta\mathcal{T}}{\mathcal{T}} = c \cdot \frac{T_x - T_z}{T_x + T_z} \cdot \int_0^{\pi} \pi f(\theta)(3\cos^2\theta - 1)\sin\theta d\theta, \quad (1)$$

where $\Delta\mathcal{T}$ and $\mathcal{T}$ is the difference and the average of the transmitted intensities for the two polarizations, respectively. The factor c expresses linear scaling with the concentration. The wavelength dependence emerges in the second term through the transmission anisotropy of individual crystals, while the integral captures the field dependence, hereafter referred to as $\Phi(B)$, describing the degree of the magnetic alignment[39].

The universal field dependence shown in Fig. 4 was fitted by numerically evaluating $\Phi(B)$ for different values of the magnetic anisotropy using a typical crystal size of V=200×200×700 nm^3. We found the best fitting with $M_x/M_z = 1.11 \pm 0.04$ in good agreement with the value obtained from the magnetization study on oriented samples at room temperature. As the difference of the experimental and the fitted curves are likely due to the size-distribution of the crystals, we refined the fit assuming lognormal distribution of the crystal size. To reduce the number of free parameters, we fixed the average length of the crystals and the magnetization anisotropy to the values previously obtained by the single-size-fit, i.e. L=700 nm and $M_x/M_z = 1.1$. Then, we obtained 220 nm for the standard deviation of the length and 8:2 for the aspect ratio of the crystals. These are both realistic in the light of scanning electron micrographs (aspect ratio of 7:2 was considered in the single-size-fit) and further improved the quality of the fit.

Spectral features of the MLD effect in hemozoin. To gain more insight into the microscopic optical properties of hemozoin and trace the spectral range optimal for diagnosis, we studied MLD effect from the ultraviolet to the near-infrared region (λ=300-1300 nm) in B=0.3 T. We also investigated the influence of different suspension media, including normal saline, blood plasma and blood, on the detectability of hemozoin.

As shown in Fig. 5 the MLD spectra of hemozoin suspensions in saline and blood plasma are essentially iden-

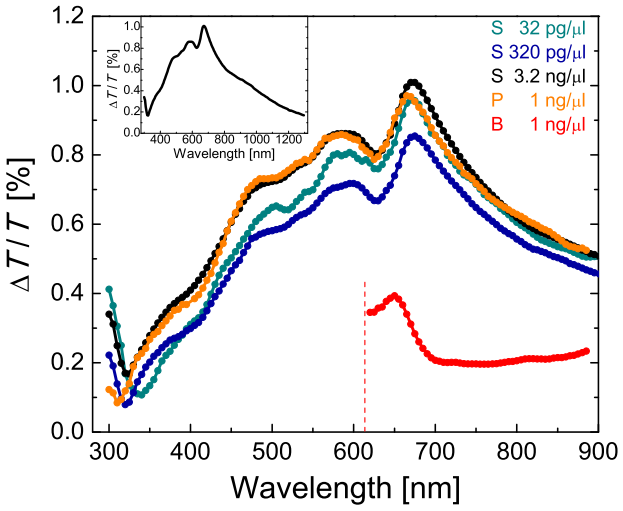

FIG. 5: | **Wavelength dependence of the MLD effect in hemozoin suspensions.** MLD spectra for room-temperature hemozin suspensions in normal saline (S), blood plasma (P) and full blood (B) normalized to a concentration of 1 ng/μl. The inset shows the MLD effect over a broader spectral range in normal saline.

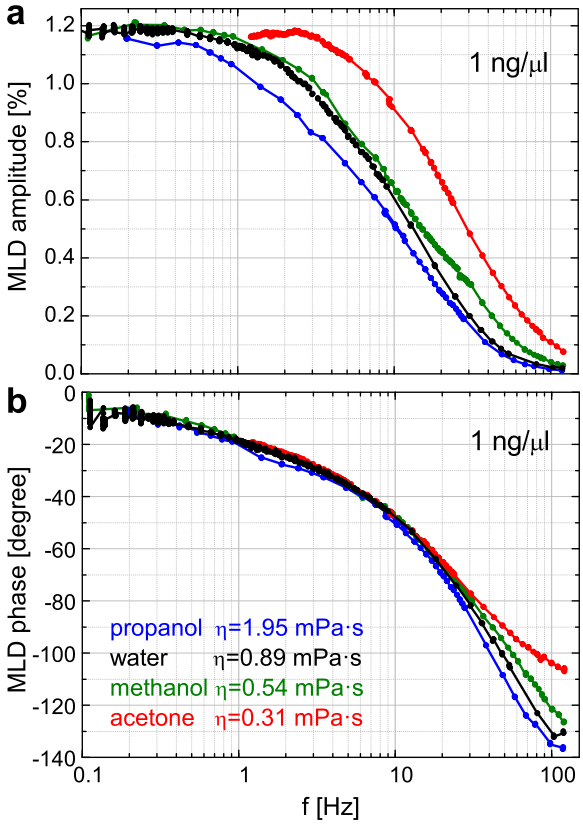

FIG. 6: | **Magnetically driven dynamics of hemozoin crystals in various suspension media at room temperature.** (**a**)/(**b**) Semi-logarithmic plot of MLD amplitude/phase versus the frequency of the field rotation, f, for hemozoin suspended in propanol, water, methanol and acetone with 1 ng/μl concentration. Results in hemolyzed blood are essentially identical with those obtained in water and not shown here. Viscosity (η) for the different media are also indicated.

tical and exhibit characteristic peaks distributed mostly over the visible range, which may serve as optical fingerprints of malaria pigment. These peaks are likely dominated by the linear dichroism of absorption bands observed over the same range[32,37]. The magnitude of MLD spectra shows linear dependence on the hemozoin content over a wide range of concentrations reassuring the feasibility of a quantitative diagnosis. The effect is the largest at $\lambda\approx$670 nm, where the macroscopic transmission anisotropy reaches $\Delta\mathcal{T}/\mathcal{T}$=1% for the suspension with 1 ng/μl hemozoin content corresponding to an optical path of d=10 mm. If we assume that only the absorption of the crystals contribute to MLD, i.e. polarization dependent light scattering can be neglected, this value corresponds to a robust transmission anisotropy $\frac{T_x-T_z}{T_x+T_z}\approx$40% for a typical crystal and a large difference in its absorption coefficients $\Delta\alpha=\alpha_z-\alpha_x\approx 1.5\cdot10^4\,\mathrm{cm}^{-1}$.

The MLD effect decreases in blood by a factor of ~3. The overall sensitivity is further reduced owing to strong absorption and light scattering by the blood components, mainly by red blood cells. For wavelengths shorter than ~620 nm the transmitted intensity drastically drops allowing no further observation of the MLD signal. To approach the sensitivity level achieved for blood plasma by visible light, we used hemolyzed blood in following studies, which helps to strongly reduce light scattering. Please note that the hemolysis of actually infected blood samples is also favourable for the diagnosis, since the hemozoin portion still contained within the erythrocytes can be released into the blood plasma, hence becoming effectively detectable this way. We also work on the development of simple techniques for the separation of hemoglobin from hemolyzed blood, while keeping hemozoin within the plasma, and on the selective filtering of hemozoin[40].

Malaria pigment crystals as magnetic micro-rotors. For a sensitive detection of weak polarization effects generated by low amounts of hemozoin in infected blood, it is inevitable to use polarization modulation as was already proposed by Newman and coworkers[17] and also applied in our magneto-optical experiments. However, besides polarization modulation of the probing light, – in the special case of hemozoin crystals – also magnetic modulation of light polarization is conceivable.

The central idea is that the magnetically aligned crystallites follow the direction of a rotating magnetic field, i.e. they behave as magnetically driven micro-rotors in a suspension. Moreover, the dichroic planes of the crystals rotate in a synchronous manner, thus the suspension acts as a spinning polarizer modulating the intensity and the polarization of the transmitted light beam. The application of a polarizing beam splitter after the sample and the differential detection of the two orthogonally po-

larized beams by a balanced photodiode-bridge provide an efficient scheme for the reduction of intensity noise, meaning that an ordinary laser diode is sufficient as light source. From the differential signal the a.c. component corresponding to the second harmonic of the rotation frequency is selectively detected, which originates solely from MLD caused by the rotation of the dichroic crystals and it is not affected by parasitic intensity noise coming from optical, mechanical and thermal instability of the device.

A special arrangement of permanent magnets in a ring-shaped structure surrounding the sample, called Halbach-cylinder[41], is used to generate a uniform magnetic field of B=1 T at the sample position. The ring is rotated by a d.c. electric motor with a frequency adjustable over the range of f=0.1-130 Hz, resulting in a field which rotates within the plane perpendicular to the light path. We found that the efficient co-alignment of the crystals using the strong and nearly homogeneous magnetic field of the Halbach-cylinder rotated with fairly large frequencies plays crucial role in the sensitivity of our method and leads significant improvements over previous magneto-optical detection schemes[17,18]. (For further details on the device see Methods section).

Applying this new methodology, we carried out a phase-sensitive detection of MLD on hemozoin suspensions. Besides the amplitude of the signal, its time delay relative to the rotating field has also been recorded. To understand the dynamics of the crystals, we measured the frequency dependence of MLD over f=0.1-130 Hz in solvents with different viscosity (see Fig. 6). The amplitude of MLD remains constant at low frequencies, then decays drastically towards higher frequencies. The phase shift of MLD grows gradually with increasing frequency with a viscosity dependence exposed more in the high-frequency region.

These results can be understood via the basic features of the highly complex crystal dynamics as schematically shown in Figs. 2c-e. In a strong static field, as in Fig. 2c, the hard axes of the crystallites are distributed uniformly in the plane perpendicular to the field direction. Upon the rotation of this field, the resulting torque forces the hard axes of the crystals to precess around the rotation axis and follow the field. Due to the viscosity of the fluid the system behaves as an ensemble of damped rotators. Consequently, towards higher frequencies the crystals experience an increasing angular delay relative to the field and their hard axes tend to align parallel to the rotation axis. This manifests in the finite phase and the decreasing amplitude of MLD, respectively. When this alignment is completed, no magnetic torque acts on the crystals as the magnetic field rotates within their easy planes, hence they stop moving. The analysis of rotational dynamics for easy-axis and easy-plane magnetic particles has recently been subject to extensive theoretical and experimental research[42–44]. The dynamics described here is specific to crystals with easy-plane magnetic anisotropy as was also reported for other easy-plane paramagnetic particles[42,44,45] and fundamentally differs from the motion of easy-axis crystallites. In the present easy-plane situation, MLD signal is suppressed towards high frequencies because optically isotropic planes of the dynamically co-aligned crystals are exposed to the light and consequently no dichroism can emerge.

We tested the concentration threshold of hemozoin detection achievable by this method. Frequency dependence of MLD was measured for aqueous suspensions of hemozoin prepared over six orders of magnitude in concentration, namely from 30 ng/μl to 0.5 pg/μl. MLD curves displayed in Figs. 7a-b show that the lowest concentration corresponding to a parasitemia less than 1 parasite/μl is still readily detectable. More relevant to diagnosis, our current detection limit for hemozoin in blood is c=15 pg/μl as demonstrated in Figs. 7c-d. This exceeds the performance of RDTs and approaches the detection limit achievable by microscopic observation of infected blood. In order to sufficiently reduce the strong light scattering of red blood cells over the visible range, the experiments were carried out in hemolyzed blood (see Methods section). Please note, that the concentration values in Figs. 7c-d correspond to hemozoin contents in full blood and not in hemolyzed blood obtained by 20-fold dilution with distilled water. Thus, we can conclude that the sensitivity of the detection in hemolyzed blood is close to that in water. The precision of the hemozoin content for the series of blood samples was checked by the parallel measurement of MLD signal on water with the same hemozoin concentrations. At the moment the threshold of our detection is not limited by the signal-to-noise ratio of MLD but by a mainly frequency independent baseline superimposed on the signal. This weak contribution to the second-harmonic signal may come e.g. from the Voigt effect of the medium. The reproducibility of the lowest-concentration data together with the baseline measured for blood sample containing no hemozoin are displayed in the inset of Figs. 7c.

Discussion

By combining magnetization measurements, broadband magneto-optical spectroscopy and electron transmission microscopy we determined quantitatively the magnetic and optical anisotropy characteristic to submicron-sized single crystals of hemozoin. Based on these results we refined previous models describing the magnetic alignment of the crystals in suspensions[17,18]. These fundamental properties offer a unique path for the magnetic manipulation and optical detection of these crystallites and are also relevant to the development of new drugs blocking hemozoin production. Dielectric anisotropy may also play role in the co-alignment of hemozoin crystallites during their nucleation within the digestive vacuoles of the parasites[35].

We studied the dynamics of the crystals during their magnetically driven rotation in suspensions with differ-

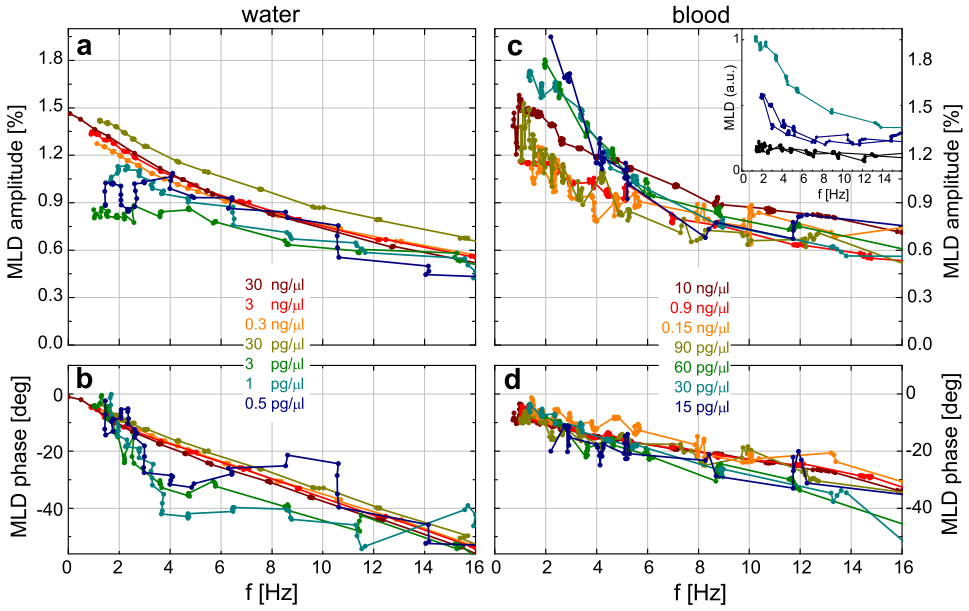

FIG. 7: | **Sensitivity of the optical diagnostic method based on the magnetic rotation of hemozoin crystals in water and blood.** (**a**)/(**b**) MLD amplitude/phase for hemozoin in water over a limited frequency range optimal in sense of signal to noise ratio. (**c**)/(**d**) MLD amplitude/phase for hemozoin in blood over the same frequency range. The concentration of hemozoin varies over five and three orders of magnitude in water and blood, respectively. The amplitude of the MLD signal is normalized to 1 ng/μl hemozoin content. Concentrations of blood samples refer to the hemozoin contents in full blood and not in hemolyzed blood. The concentration levels of 0.5 pg/μl and 15 pg/μl are still readily detectable in water and blood, respectively. Inset in panel (**c**) shows the reproducibility for the baseline (black curves) and the lowest-concentration data (with color coding used in the main panel).

ent viscosity including hemolyzed blood. Based on the fact that the synchronous motion of such micro-rotors induces intensity modulation of the transmitted light via polarization effects, we assembled a device for the detection of malaria pigment in blood. The device provides a more sensitive way of diagnosis RDTs and approaches the sensitivity achievable by microscopic observation of infected red blood cells, which is the most effective diagnosis in practice to date. We found that the sensitivity of the hemozoin detection in blood plasma is even higher and we are aiming at the improvement of the detection threshold by filtration techniques.

We expect no major reduction of sensitivity for infected blood samples compared to the threshold reported here for synthetic hemozoin in blood for the following reasons. First, hemolysis of infected blood helps to release the portion of hemozoin still contained within the erythrocytes into the blood plasma. Furthermore, our preliminary data indicate that the magnitude of MLD signal – observed in large fields (B$\gtrsim$1 T) rotating with low frequencies – shows only moderate changes with crystal size and morphology in agreement with previous results[17]. On the other hand, the frequency dependence of both the amplitude and phase of MLD may provide information specific to the type of the parasites as increasing crystal size results in a shift of the decay frequency towards higher values. Nevertheless, both the detection threshold of our device and its specificity to different parasites need to be proved via extensive clinical tests.

The use of hemozoin as the marker compound for detecting Plasmodium infections has clear advantages over the currently used RDTs. The production of hemozoin is a defense reaction on behalf of the parasite that transforms a host protein into a magnetically detectable compound with physico-chemical properties invariable upon genetic variations of the parasites. Therefore, efficiency of our method is not affected by high rates of their genetic variation. In contrast, performance of the antigen-based diagnostics relies on the antigen-antibody reaction which may be perturbed upon mutations in the antigen. From this respect, it is important to emphasize that Plasmodium strains are known to show great variability of their proteins[46,47], thereby potentially jeopardizing the efficiency of recognition by a highly specific antibody developed for a rapid diagnostic test.

Beyond the scope of malaria research and diagnosis, our results can contribute to biomedical applications of optically and/or magnetically anisotropic submicron-sized particles[48–52]. We believe that the magnetic micro-rotor concept recognized specifically for malaria pigment crystals can be generally applied for the magnetic control, manipulation and detection of submicron-sized magnetic particles functionalized to interact with biomolecules and cells as it has already been demonstrated e.g. in the study of the elastic properties of single DNA molecules using magnetic beads[53].

Recently, various applications of rotating magnetic field has also been proposed in material sciences. These include the three dimensional alignment of magnetically anisotropic micro-particles aiming to produce magnetically oriented microcrystal arrays for X-ray crystallography[54] or to reinforce composites by superparamagnetic platelets[45]. Rotating magnetic fields have also been applied for investigating the formation and rotational dynamics for chains of paramagnetic beads[55–57]. Our method enables the rotation of strong magnetic fields – also characterized by a high level of homogeneity over a large sample volume – at frequencies ranging from 0.1-130 Hz, while the polarization detection scheme supports monitoring of the dynamics even when magnetic particles are present at ppm concentrations in solution. Thus, this methodology can help to improve the performance in the applications mentioned above.

Methods

Preparation and characterization. Hemozoin crystals were synthetized following the aqueous acid-catalyzed method described by M. Jamarillo and coworkers[28]. Hemin was dissolved in NaOH with the dropwise addition of propionic acid adjusting a pH value of approximately 4. After annealing the mixture for 18 hours at 70 °C, the crystals were separated and washed with $NaHCO_3$, MilliQ water and MeOH, multiple times, alternately – as prescribed by the authors. According to our TEM measurements the typical size of the crystals obtained by this method is approximately $200\times200\times700\,\mathrm{nm}^3$.

The transmission electron micrographs were obtained by using two different methods for the fixation of crystals. To avoid aggregation of the crystals, in both cases the suspensions were prepared with hemozoin contents $< 10\,\mu\mathrm{g}/\mu\mathrm{l}$ and long-term ultrasonication. The aqueous suspension of hemozoin crystals was dropped onto formvar membrane (purchased from Sigma-Aldrich) placed on 200 mesh copper grid and dried at room temperature. The other method applied for magnetically aligned ensembles of crystals was freeze-fracture. In this case the suspension medium was a mixture of 70% water and 30% glycerol to prevent the formation of ice crystals. The droplets (1-2 μl) of suspension were pipetted on a gold specimen holder kept in a field of B=0.5 T at room temperature for 30 s, then plunged into partially solidified Freon for 20 s freezing and then placed and stored in liquid nitrogen. Fracturing was carried out at 173 K in a Balzers Freeze-fracture Device (Balzers BAF 400 D). The fractured faces were etched for 30 s at 173 K. The replicas, prepared by platinum-carbon shadowing, were cleaned and washed with distilled water. The membranes and replicas obtained by the two methods were examined in a transmission electron microscope as shown in Fig. 1 and Fig. S1, respectively.

For experiments performed on hemozoin crystals suspended in blood plasma and hemolyzed blood, the blood plasma was obtained via the centrifugation of blood samples and hemolysis of blood was achieved by 20-fold dilution of blood with distilled water. Freshly drawn blood was acquired from healthy volunteers.

Magnetization measurements. Magnetization measurements on suspensions were performed using a Superconducting Quantum Interference Device (SQUID) in magnetic fields ranging from B=0 to 5 T at temperatures T=2-300 K. Powder samples were measured over a broader field range B=0-9 T using a magnetometer with a.c. pick-up coil. The magnetization component parallel to the applied magnetic field was detected. Liquid samples were placed in hermetically closed plastic straws, while gelatine capsules were used in the case of the solid powder samples. The diamagnetic baselines originating from the sample holders and the suspension medium were measured separately and subtracted from the data.

Magneto-optical methodology. The spectrometer capable of the measurement of MLD over the wavelength range of λ=180-1300 nm was assembled using a triple grating monochromator, broad-band light sources (Xe-arc and tungsten lamps) together with a photomultiplier and an InGaAs photodiode as detectors. The experiment was set up in Voigt configuration, that is the magnetic field was applied perpendicularly to the direction of the light propagation. Light beam after the sample was collected using lenses with typical numerical aperture of NA=0.1-0.2. The fast switching between the light polarizations parallel and perpendicular to the magnetic field was carried out with a fused silica photoelastic modulator operating at a frequency of 50 kHz[58]. In order to eliminate linear polarization effects other than MLD, the zero-field baseline was measured and subtracted from the finite-field data.

Diagnostic method and instrumentation. The principles of the new technique have been described in the main text. Figure 8 provides a schematic representation of the diagnostic setup.

Derivation of MLD effect for suspensions. As discussed in the main text, the magnetic and optical properties of hemozoin crystals are characterized by an axial anisotropy. Hence, the value of the complex transmission coefficient for light polarization parallel to the C_{4v} axis (z-axis) of a crystal differs from the values corresponding to polarizations within the perpendicular plane (xy-plane), i.e. $t_z \neq t_x = t_y$. The same difference holds for the magnetization in external magnetic fields pointing along the z-axis or lying in the xy-plane as $M_z \neq M_x = M_y$.

While the matrix of the transmission coefficients, $\hat{t}$, is diagonal for each crystal in its own xyz frame, the transmission of the whole suspension needs to be calculated in a common $x'y'z'$ reference frame, where y'- and z'-axis are conveniently chosen as the direction of the light propagation and the magnetic field, respectively. The new form of the transmission matrix, $\hat{t}'$ – for a crystal with its z-axis pointing in the direction defined by the azimuth angle, θ and polar angle, ϕ in the $x'y'z'$ frame

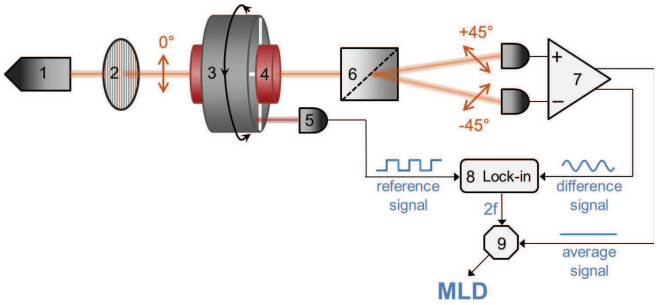

FIG. 8: | **Flowchart of the diagnostic setup.** The beam from the laser diode (1) passes through a polarizer (2) and becomes vertically polarized. Then it goes through the sample holder (4) located in the bore of the Halbach magnet (3). The magnet is rotated with a frequency f by a d.c. motor, thus, the uniform magnetic field of B≈1 T at the sample position rotates within the plane perpendicular to the light propagation. After the sample, the beam is divided into two parts with orthogonal polarizations ($\pm 45^o$) by a Rochon prism (6). The difference and the average of their intensities are detected by a balanced photodiode bridge (7). The $2f$ component of the difference signal is filtered out by a lock-in amplifier (8) using the reference signal from an optoswitch (5) monitoring the rotation of the magnet. To obtain the MLD signal, the amplitude of the second harmonic ($2f$) signal is normalized with the average signal by a divisor (9).

– can be obtained by the corresponding base transformation. In this common frame, the portion of the light intensity transmitted by the crystal for polarization along the x'/z' direction is given by $T_{x'/z'} = \left|\hat{t}' \cdot \mathbf{e}_{\mathbf{x}'/\mathbf{z}'}\right|^2$, where $\mathbf{e}_{\mathbf{x}'}$ and $\mathbf{e}_{\mathbf{z}'}$ are unit vectors pointing along the x'- and z'-axis, respectively.

For an ensemble of the crystals, the macroscopic linear dichroism exhibited by the suspension is obtained by averaging over the contributions from individual crystallites according to $\frac{\Delta\mathcal{T}}{\mathcal{T}} = c \cdot \frac{T_x - T_z}{T_x + T_z} \cdot \int_0^\pi \pi f(\theta)(3\cos^2\theta - 1)\sin\theta d\theta$, where $T_x = |t_x|^2$ and $T_z = |t_z|^2$. The distribution of the azimuth angle is governed by the Boltzmann factor: $f(\theta) = \frac{e^{-U/k_B T}}{2\pi \int_0^\pi e^{-U/k_B T}\sin\theta d\theta}$. The angular distribution is independent of the polar angle, since the full rotational symmetry around the magnetic field is preserved. Assuming a linear field dependence of the magnetization, which is experimentally confirmed at room temperature, the magnetic anisotropy energy is $U = -\frac{1}{2}\frac{B^2}{\mu_0} cos^2(\theta)(\chi_{zz} - \chi_{xx})V$. Here, χ_{zz} and χ_{xx} stand for the linear magnetic susceptibility of a crystal along the hard axis and within the easy plane, respectively. The typical volume of a crystal, V, is approximated as $200 \times 200 \times 700\,\mathrm{nm}^3$ according to TEM images. The field dependence of $\frac{\Delta\mathcal{T}}{\mathcal{T}}$ was evaluated numerically and used for the fitting of the MLD data with two free parameters. The first parameter is a scale factor, from which we could obtain the transmission anisotropy of a single crystal, $\frac{T_x - T_z}{T_x + T_z}$, as a function of the wavelength. The other parameter is $(\chi_{zz} - \chi_{xx})V$, which determines the distribution of the azimuth angle via the magnetic anisotropy energy, hence, it is the only parameter describing the universal field dependence of MLD. Considering an average crystal volume of $V = 2.8 \cdot 10^{-20}\,\mathrm{m}^3$, the difference in the magnetization densities is directly obtained.

Numerical calculation of magnetization. As argued in the main text, the magnetic behaviour of Fe^{3+} ions with S=5/2 spins in hemozoin is described by the following axially symmetric Hamiltonian: $H = D\left(S_z^2 - \frac{S(S+1)}{3}\right) + \mu_B g \mathbf{BS}$. For a given set of {D, **B**}, we determined the energy eigenvalues (ε_n) by the numerical diagonalization of this 6×6 matrix. Then, the magnetization density vector was obtained according to $\mathbf{M} = \frac{1}{V} k_B T \frac{\partial}{\partial \mathbf{B}} ln Z$, where Z is the partition function in the grand canonical ensemble, $Z = \left(\sum_n e^{-\varepsilon_n / k_B T}\right)^N$. Due to the magnetocrystalline anisotropy, the energy eigenvalues depend not only on the strength of the magnetic field but also on its orientation relative to the crystal (θ). For comparison with the experimental data, only the component of the magnetization vector parallel to the field direction was considered.

Besides the principal values M_x and M_z, the magnetization density of unordered samples were also evaluated by averaging over the contributions from individual crystals: $\langle M \rangle = \frac{1}{4\pi}\int_0^\pi 2\pi[M_x(B_x)\sin\theta + M_z(B_z)\cos\theta]\sin\theta d\theta$. M_x and $\langle M \rangle$ were respectively measured on oriented and random hemozoin suspensions in a mixture of 70% water and 30% glycerol. In the former case we used a field-cooled freezing procedure. The experimental data, both the field and the temperature dependent magnetization curves, were fitted using the single-ion anisotropy factor (D) as the only fitting parameter.

The good correspondence between the values of axial anisotropy found in the present magnetization experiments and reported by former EPR[25] and Mössbauer[24] spectroscopic studies implies that in paramagnetic hemozoin crystals magnetocrystalline anisotropy dominates over the shape anisotropy unlike in usual ferro- and ferrimagnetic crystals with micron or submicron size. This is further supported by TEM images recorded from cleaved surfaces of field-cooled suspensions as presented in the Supplementary Information.

[1] World malaria report 2011, December 13, 2011. (http://www.who.int/malaria).
[2] Greenwood, B.M., Bojang, K., Whitty, C.J., Targett, G.A. Malaria, *Lancet* **365**, 1487–1498 (2005).
[3] Yuan, J., Cheng, K.C., Johnson, R.L., Huang, R., Pattaradilokrat, S., Liu, A., Guha, R., Fidock, D.A., Inglese,

J., Wellems, T.E., Austin, C.P. and Su, X. Chemical genomic profiling for antimalarial therapies, response signatures, and molecular targets, *Science* **333**, 724−729 (2011).

[4] Bell, D., Wongsrichanalai, C. and Barnwell, J.W. Ensuring quality and access for malaria diagnosis: how can it be achieved? *Nat. Rev. Microbiol.* **4**, 682−695 (2006).

[5] Moody, A. Rapid diagnostic tests for malaria parasites, *Clin. Microbiol. Rev.* **15** 66−78 (2002).

[6] Wilson, M.L. Malaria rapid diagnostic tests, *Clin. Inf. Dis.* **54**, 1637−1641 (2012).

[7] Murray, C.K. and Bennett, J.W. Rapid Diagnosis of Malaria, *Interdiscip. Perspect. Infect. Dis.* **2009**, 415953 (2009).

[8] Gamboa, D., Ho, M-F., Bendezu, J., Torres, K., Chiodini, P.L., Barnwell, J.W., Incardona, S., Perkins, M., Bell, D., McCarthy, J. and Cheng, Q. A Large Proportion of P. falciparum Isolates in the Amazon Region of Peru Lack pfhrp2 and pfhrp3: Implications for Malaria Rapid Diagnostic Tests *PLoS ONE* **5**, e8091 (2010).

[9] Rock, E.P., Marsh, K., Saul, A.J., Wellems, T.E., Taylor, D.W., Maloy, W.L. and Howard, R.J. Comparative analysis of the Plasmodium falciparum histidine-rich proteins HRP-I, HRP-II and HRP-III in malaria parasites of diverse origin, *Parasitology* **95**, 209−227 (1987).

[10] Andrade, B.B., Reis-Filho, A., Barros, A.M., Souza-Neto, S.M., Nogueira, L.L., Fukutani, K.F., Camargo, E.P., Camargo, L.M., Barral, A., Duarte, A. and Barral-Netto, M. Towards a precise test for malaria diagnosis in the Brazilian Amazon: comparison among field microscopy, a rapid diagnostic test, nested PCR, and a computational expert system based on artificial neural networks, *Malaria J.* **9**, 117 (2010).

[11] Khairnar, K., Martin, D., Lau, R., Ralevski, F. and Pillai D.R. Multiplex real-time quantitative PCR, microscopy and rapid diagnostic immuno-chromatographic tests for the detection of Plasmodium spp: performance, limit of detection analysis and quality assurance, *Malaria J.* **8**, 284 (2009).

[12] Zimmerman, P.A., Thomson, J.M., Fujioka, H., Collins, W.E. and Zborowski, M. Diagnosis of malaria by magnetic deposition microscopy, *Am. J. Trop. Med. Hyg.* **74**, 568−572 (2006).

[13] Bélisle, J.M., Costantino, S., Leimanis, M.L., Bellemare, M.-J., Bohle, D.S., Georges, E. and Wiseman, P.W. Sensitive detection of malaria infection by third harmonic generation imaging, *Biophys. J.* **94**, L26−L28 (2008).

[14] Yatsushiro, S., Yamamura, S., Yamaguchi, Y., Shinohara, Y., Tamiya, E., Horii, T., Baba, Y. and Kataoka, M. Rapid and highly sensitive detection of malaria-infected erythrocytes using a cell microarray chip, *PloS ONE* **5**, e13179 (2010).

[15] Samson, E.B., Goldschmidt, B.S., Whiteside, P.J.D., Sudduth, A.S.M., Custer, J.R., Beerntsen, B. and Viator, J.A. Photoacoustic spectroscopy of β-hematin, *J. Opt.* **14**, 065302 (2012).

[16] Kim, C.C., Wilson, E.B. and DeRisi, J.L. Improved methods for magnetic purification of malaria parasites and haemozoin, *Malaria J.* **9**, 17 (2010).

[17] Newman, D.M., Heptinstall, J., Matelon, R.J., Savage, L., Wears, M.L., Beddow, J., Cox, M., Schallig, H.D.F.H. and Mensz P.F. A magneto-optic route toward the in vivo diagnosis of malaria: preliminary results and preclinical trial data, *Biophys. J.* **95**, 994−1000 (2008).

[18] Mens, P.F., Matelon, R.J., Nour, B.Y.M., Newman, D.M. and Schallig, H.D.F.H. Laboratory evaluation on the sensitivity and specificity of a novel and rapid detection method for malaria diagnosis based on magneto-optical technology (MOT), *Malaria J.* **9**, 207 (2010).

[19] Castilho, M.S., Laube, T., Yamanaka, H., Alegret, S. and Pividori, M.I. Magneto immunoassays for Plasmodium falciparum histidine-rich protein 2 related to malaria based on magnetic nanoparticles, *Anal. Chem.* **83**, 5570−5577 (2011).

[20] Yuen, C., Liu, Q. Magnetic field enriched surface enhanced resonance Raman spectroscopy for early malaria diagnosis, *J. Biomed. Opt.* **17**, 017005 (2012).

[21] Goldberg, D.E., Slater, A.F.G., Cerami, A. and Henderson, G.B. Hemoglobin degradation in the malaria parasite Plasmodium falciparum: An ordered process in a unique organelle, *Proc. Natl. Acad. Sci. USA* **87**, 2931−2935 (1990).

[22] Gluzman, I.V., Francis, S.E., Oksman, A., Smith, C.E., Duffin, K.L and Goldberg, D.E. Order and specificity of the Plasmodium falciparum hemoglobin degradation pathway, *J. Clin. Invest.* **93**, 1602−1608 (1994).

[23] Slater, A.F.G., Swiggard, W.J., Orton, B.R., Flitter, W.D., Goldberg, D.E., Cerami, A. and Henderson, G.B. An iron-carboxylate bond links the heme units of malaria pigment, *Proc. Natl. Acad. Sci. USA* **88**, 325−329 (1991).

[24] Bohle, D.S., Debrunner, P., Jordan, P.A., Madsen, S.K. and Schulz C.E. Aggregated heme detoxification byproducts in malarial trophozoites: β−hematin and malaria pigment have a single S=5/2 iron environment in the bulk phase as determined by EPR and magnetic Mössbauer spectroscopy, *J. Am. Chem. Soc.* **120**, 8255-8256 (1998).

[25] Sienkiewicz, A., Krzystek, J., Vileno, B., Chatain, G., Kosar, A.J., Bohle, D.S. and Forró, L. Multi-frequency high-field EPR study of iron centers in malarial pigments, *J. Am. Chem. Soc.* **128**, 4534−4535 (2006).

[26] Walczak, M., Lawniczak-Jablonska, K., Sienkiewicz, A., Demchenko, I.N., Piskorska, E., Chatain, G. and Bohle, D.S. Local environment of iron in malarial pigment and its substitute β−hematin, *Nucl. Instrum. Meth. B* **238**, 32−38 (2005).

[27] Hanscheid, T., Egan, T.J. and Grobusch, M.P. Haemozoin: from melatonin pigment to drug target, diagnsotic tool, and immune modulator. *Lancet Infect. Dis.* **7**, 675−685 (2007).

[28] Jaramillo, M., Bellemare, M.J., Martel, C., Shio, M.T., Contreras, A.P., Godbout, M., Roger, M., Gaudreault, E., Gosselin, J., Bohle, D.S. and Olivier, M. Synthetic plasmodium-Like hemozoin activates the immune response: A morphology - function study, *PLoS ONE* **4**, e6957 (2009).

[29] Pagola, S., Stephens, P.W., Bohle, D.S., Kosar, A.D. and Madsen, S.K. The structure of malaria pigment β-haematin, *Nature* **404**, 307−310 (2000).

[30] Noland, G.S., Briones, N. and Sullivan Jr., D.J. The shape and size of hemozoin crystals distinguishes diverse Plasmodium species, *Mol. Biochem. Parasit.* **130**, 9199 (2003).

[31] Oliveiraa, M.F., Kyciab, S.W., Gomezb, A., Kosarc, A.J., Bohlec, D.S., Hempelmannd, E., Menezese, D., Vannier-Santose, M.A., Oliveiraa, P.L. and Ferreira, S.T. Structural and morphological characterization of hemozoin produced by Schistosoma mansoni and Rhodnius prolixus, *FEBS Lett.* **579**, 610−616 (2005).

[32] Bohle, D.S. and Helms, J.B. Synthesis of β−hematin by dehydrohalogenation of hemin, *Biochem. Bioph. Res. Co.*

193, 504−508 (2003).

[33] Frosch, T., Koncarevic, S., Zedler, L., Schmitt, M., Schenzel, K., Becker, K. and Popp J. In situ localization and structural analysis of the malaria pigment hemozoin, *J. Phys. Chem. B* **111**, 11047−11056 (2007).

[34] Buller, R., Peterson, M.L., Almarsson, Õ. and Leiserowitz, L. Quinoline binding site on malaria pigment crystal: a rational pathway for antimalaria drug design, *Cryst. Growth. Des.* **2**, 553562 (2002).

[35] Kapishnikov, S., Berthing, T., Hviid, L., Dierolf, M., Menzel, A., Pfeiffer, F., Als-Nielsen, J. and Leiserowitz L. Aligned hemozoin crystals in curved clusters in malarial red blood cells revealed by nanoprobe X-ray Fe fluorescence and diffraction, *Proc. Natl. Acad. Sci. USA* **109**, 1118411187 (2012).

[36] Eaton, W.A., Hanson, L.K., Stephens, P.J., Sutherland, J.C. and Dunn, J.B.R. J. Optical spectra of oxy- and deoxyhemoglobin *J. Am. Chem. Soc.* **100**, 4991−5003 (1978).

[37] Wood, B.R., Langford, S.J., Cooke, B.M., Lim, J., Glenister, F.K., Duriska, M., Unthank, J.K. and McNaughton, D. Resonance Raman spectroscopy reveals new insight into the electronic structure of β-hematin and malaria pigment, *J. Am. Chem. Soc.* **126**, 9233−9239 (2004).

[38] Newman, D.M., Matelon, R.J., Wears, M.L., Savage, L., Heptinstall, J., Beddow, J. and Cox, M. Magneto-Optics in the Service of Medicine - Diagnosis via the Cotton-Mouton Effect-, *PhotonicsGlobal@Singapore, 2008. IPGC 2008. IEEE*, 1−3 (2008).

[39] Langevin, P. Magnetisme et theorie des electrons, *CR Acad. Sci. Paris* **151**, 331368 (1910).

[40] Butykai, A. *et al.* to be published.

[41] Halbach, K. Design of permanent multipole magnets with oriented rare earth cobalt material, *Nucl. Instrum. Methods* **169**, 1−10 (1980).

[42] Erb, R.M., Segmehl, J., Charilaou, M., Leoffler J.F. and Studart A.R. Non-linear alignment dynamics in suspensions of platelets under rotating magnetic fields, *Soft Matter*, **8**, 76047609, (2012).

[43] Tierno, P., Claret, J. and Sagus, F. Overdamped dynamics of paramagnetic ellipsoids in a precessing magnetic field, *Phys. Rev. E* **79**, 021501 (2009).

[44] Dhar, P., Swayne, C.D., Fischer, T.M., Kline, T. and Sen A. Orientations of over damped magnetic nano-gyroscopes, *Nano Lett.* **7**, 1010-1012 (2007).

[45] Erb, R.M., Libanori, R., Rothfuchs N. and Studart, A.R. Fields Composites Reinforced in Three Dimensions by Using Low Magnetic Fields, *Science* **335**, 199 (2012).

[46] Mackinnon, M.J. and Marsh, K. The selection landscape of malaria parasites, *Science* **328**, 866-871 (2010).

[47] Templeton, T.J. The varieties of gene amplification, diversification and hypervariability in the human malaria parasite, Plasmodium falciparum, *Mol. Biochem. Parasit.* **166**, 109-116 (2009).

[48] Koumura, N., Zijlstra, R.W.J., van Delden, R.A., Harada, N. and Feringa, B.L. Light-driven monodirectional molecular rotor, *Nature* **401**, 152-155 (1999).

[49] Kuimova, M.K., Botchway, S.W., Parker, A.W., Balaz, M., Collins, H.A., Anderson, H.L., Suhling, K. and Ogilby, R. Imaging intracellular viscosity of a single cell during photoinduced cell death, *Nat. Chem.* **1** 69−73 (2009).

[50] Di Leonardo, R., Búzás, A., Kelemen, L., Vizsnyiczai, G., Oroszi, L. and Ormos, P. Hydrodynamic Synchronization of Light Driven Microrotors, *Phys. Rev. Lett.* **109**, 034104 (2012).

[51] Dharmadhikari, J.A., Roy, S., Dharmadhikari, A.K., Sharma, S. and Mathur, D. Naturally occurring, optically driven, cellular rotor *Appl. Phys. Lett.* **85**, 6048−6050 (2004).

[52] Dasgupta, R., Ahlawat, S., Verma, R.S. and Gupta P.K. Optical orientation and rotation of trapped red blood cells with Laguerre-Gaussian mode, *Opt. Express* **19**, 7680−7688 (2011).

[53] Strick, T.R., Allemand, J.-F., Bensimon, D., Bensimon, A. and Croquette, V. The Elasticity of a Single Supercoiled DNA Molecule, *Science* **271**, 1835−1837 (1996).

[54] Kimura, F., Mizutani, K., Mikami, B. and Kimura T. Single-Crystal X-ray Diffraction Study of a Magnetically Oriented Microcrystal Array of Lysozyme, *Cryst. Growth Des.* **11**, 12-15 (2011).

[55] Vuppu, A.K., Garcia, A.A. and Hayes, M.A. Video Microscopy of Dynamically Aggregated Paramagnetic Particle Chains in an Applied Rotating Magnetic Field, *Langmuir*, **19**, 8646-8653 (2003).

[56] Melle, S., Fuller, G.G. and Rubio, M.A. Structure and dynamics of magnetorheological fluids in rotating magnetic fields, *Phys. Rev. E* **61**, 4111-4117 (2000).

[57] Melle, S., Rubio, M.A., Fuller, G.G. Orientation dynamics of magnetorheological fluids subject to rotating external fields, *Int. J. Mod. Phys. B* **15**, 758-766 (2001).

[58] Sato, K. Measurement of magneto-optical Kerr effect using piezo-birefringent modulator, *Jpn. J. Appl. Phys.* **2**0, 2403−2409 (1981).

Acknowledgements We thank G. Mihaly, Y. Tokura, M. Kellermayer and Sz. Osváth for fruitful discussions. This work was supported by Hungarian Research Funds OTKA PD75615, CNK80991, CNK81056, Bolyai 00256/08/11, TÁMOP-4.2.2.B- 10/1-2010-0009, TÁMOP-4.2.1.B-09/1/KMR-2010-0001, and ANR-NKTH ADD-MAL from National Innovation Office.

Author Contributions A.B., A.O., L.K., A.Bóta, I.K. performed the measurements; A.B., A.O., S.B., I.K. analysed the data; E. T-Sz. contributed to the sample preparation; A.B., A.O., V.K., D.Sz., I.K. developed the magneto-optical setup and the diagnostic device; A.B., A.O., I.K. wrote the manuscript; each author discussed the results; and I.K. planned and supervised the project.

Competing financial interests The authors declare no competing financial interests.